Acoustic phonon modes of rectangular quantum wires

N Nishiguchi†, Y Ando† and M N Wybourne‡

† Department of Applied Physics, Hokkaido University, Sapporo 060, Japan
‡ Department of Physics, University of Oregon, Eugene, OR 97403, USA

Abstract. Acoustic phonon modes of a free-standing rectangular quantum wire composed of cubic crystals are theoretically investigated using an algorithm developed to analyse data from resonant ultrasound spectroscopy. The normal phonon modes are classified according to their spatial symmetries into a compressional mode termed the dilatational mode and non-compressional modes referred to as the flexural, torsional, and shear modes. The formalism that we present is quite general and can be applied to wires of any cubic material. As an example, the dispersion relations are obtained for square and rectangular wires of GaAs, taking into account the anisotropic elasticity of the material. The dispersion curves for a rectangular wire are compared with those of the approximate hybrid modes referred to as the thickness and width modes, and the validity of the modes is discussed. The existence of edge modes is confirmed by examining the spatial distribution of displacement vectors.

1. Introduction

A number of theoretical and experimental studies have investigated transport phenomena in nanometre-scale wires at temperatures where the acoustic phonons are expected to show reduced-dimensional behaviour. Such behaviour is anticipated for wires whose cross-sectional dimension is less than the phonon phase-coherence length. On this length scale, phonon confinement will result in non-linear dispersion and acoustic subbands at wavevectors close to the Brillouin zone centre [1]. The effects of confinement on the phonon mean free path [2], thermal conductivity [3, 4], and phonon localization [5] have received some attention. Other work has addressed electron transport in the presence of phonon confinement. In experiments on semiconductor wires, no confinement-related effects have been found [6]. In other experiments, the resistance of metal wires was observed to change as electron energy relaxation to confined modes became possible [7, 8]. An issue related to these studies is the nature of the phonon spectrum near the zone centre. Of particular importance to wires of rectangular cross section is an understanding of edge modes, which are expected to become increasingly important as the cross-sectional dimensions of a wire are reduced.

Theoretical work on phonons in quasi-one-dimensional (Q1D) quantum wires has advanced relatively slowly, in contrast to the case for electrons in quantum wires or that of phonons in higher-dimensional systems such as superlattice structures. One of the main reasons for this is that even for rectangular wires the longitudinal acoustic (LA) and transverse acoustic (TA) wave coupling that occurs at the wire surface makes it difficult to derive the normal phonon modes and their spectra analytically. Previous theoretical approaches have been limited to specific geometries, such as circular or very flat rectangular

wires of elastically isotropic materials, and have provided only a qualitative description of the phonon dispersion in realizable quantum wires. Since the combination of the LA and TA waves depends on the geometry, frequency, and wavevector [9], it is difficult to determine the LA wave component using approximate methods. This problem has made estimates of the deformation potential scattering of electrons in wires uncertain, and has shown that to model the low-energy electron scattering rates for nanostructures accurately, a more complete treatment of the confined acoustic modes is required [10, 11].

Recently, an accurate method was developed in resonant ultrasound spectroscopy [12–14] for deriving the free vibrational modes of inhomogeneous objects. This method can treat free vibrations of a general anisotropic object with arbitrary shape as well as arbitrary mass density variation, by expanding the displacement vectors in terms of a set of basis functions that are products of powers of the Cartesian coordinates, which is called the xyz-algorithm [13]. Considering the translational symmetry of wires along the wire axis, vibrations of free-standing wires reduce to free vibrations of flakes, which can be analysed by means of the method. Thus the xyz-algorithm is found to be useful for the normal modes of free-standing wires of anisotropic materials with arbitrary-shape cross section, on suitably choosing the basis functions of the displacement vectors.

In this paper, we show that the acoustic phonon modes of Q1D wires can be precisely obtained by the xyz-algorithm. The plan of this paper is as follows. In section 2, we outline the method and apply it to a rectangular wire of a cubic material. The normal phonon modes are classified into dilatational, flexural, torsional, and shear modes, according to the symmetries of the modes. In section 3, we apply the results of section 2 to wires of the cubic semiconductor GaAs. We have chosen this material as an example because its normal modes can be compared with previously published calculations [10]. We note, however, that our approach is quite general, and can be applied to wires of any cubic material. We determine the dispersion curves and show their dependence on the cross-sectional aspect ratio. We also compare the results with previous approximate hybrid modes, termed the thickness and width modes [15, 16], calculated assuming separable boundary conditions. In section 4, we examine the spatial distribution of displacements, and show the existence of edge modes having large amplitudes at the wire corners. The normalization condition is applied to the acoustic phonon modes of rectangular wires, and the phonon field is formulated in section 5. A summary is given in section 6.

2. The method

In this section, we derive an eigenvalue equation for the acoustic phonon modes of a free-standing wire based on the variational principle. The Lagrangian of the system is given in terms of the displacement components u_i and angular frequency ω, by

$$L = \int_V \left[\frac{\rho}{2} \omega^2 u_i u_i - \frac{1}{2} C_{ijk\ell}\, \partial_i u_j\, \partial_k u_\ell \right] \, \mathrm{d}V \tag{1}$$

where ρ and $C_{ijk\ell}$ are the mass density and stiffness tensor of the constituent material. V denotes the volume of the wire. The variation of the Lagrangian δL due to the change of the displacement components $u_i \rightarrow u_i + \delta u_i$ yields

$$\delta L = \int_V \left[\rho \omega^2 u_i + \partial_j \sigma_{ji} \right] \delta u_i \, \mathrm{d}V - \int_S n_j \sigma_{ji}\, \delta u_i \, \mathrm{d}S \tag{2}$$

where n_j is the jth component of the unit vector normal to the wire surface S, and σ_{ij} is the stress tensor given by

$$\sigma_{ij} = C_{ijk\ell}\, \partial_k u_\ell. \tag{3}$$

For a free-standing wire, the stress field vanishes at the wire surface, i.e.

$$\sigma_{ij}n_j\big|_S = 0. \tag{4}$$

Considering the boundary condition (4) and postulating that the Lagrangian has a minimum with respect to u_i, we obtain the following elastic wave equation:

$$\rho\omega^2 u_i + \partial_\ell \sigma_{\ell i} = 0. \tag{5}$$

Expanding the displacement components u_i in terms of a complete set of functions $\{\Phi_\lambda\}$ as follows:

$$u_i = \chi_{i\lambda}\Phi_\lambda \tag{6}$$

and substituting equation (6) into (5), we obtain

$$\chi_{i\lambda}\rho\omega^2\Phi_\lambda + \chi_{\ell\lambda}C_{ijk\ell}\,\partial_j\partial_k\Phi_\lambda = 0. \tag{7}$$

Multiplying equation (7) by $\Phi_{\lambda'}^*$ and integrating over the volume V, we get the following generalized eigenvalue equation:

$$\chi_{i\lambda}\rho\omega^2\int_V \Phi_{\lambda'}^*\Phi_\lambda\,\mathrm{d}V - \chi_{\ell\lambda}C_{ijk\ell}\int_V \partial_j\Phi_{\lambda'}^*\,\partial_k\Phi_\lambda\,\mathrm{d}V = 0. \tag{8}$$

Defining the matrix elements $E_{i\lambda';j\lambda}$ and $\Gamma_{i\lambda';\ell\lambda}$ by

$$E_{i\lambda';j\lambda} = \delta_{i,j}\frac{\rho}{V}\int_V \Phi_{\lambda'}^*\Phi_\lambda\,\mathrm{d}V \tag{9}$$

and

$$\Gamma_{i\lambda';\ell\lambda} = \frac{C_{ijk\ell}}{V}\int_V \partial_j\Phi_{\lambda'}^*\,\partial_k\Phi_\lambda\,\mathrm{d}V \tag{10}$$

equation (8) can be expressed in a matrix form as

$$\left[\omega^2\mathbf{E} - \mathbf{\Gamma}\right]\chi = 0. \tag{11}$$

Normal phonon modes are obtained by solving equation (11). The eigenvalues ω_J^2 of equation (11) give the normal-mode spectra, and the corresponding displacement vector $\boldsymbol{u}_J$ is given by equation (6), where the coefficients $\chi_{i\lambda}$ are substituted for with the eigenvector components $\chi_{J,i\lambda}$. Here the subscript J denotes a set of quantum numbers used to specify the normal modes.

The eigenvalue equation (11) is applied to a Q1D wire of elastically anisotropic materials with arbitrary shape of the cross section. In what follows, we study acoustic phonon modes in a rectangular wire composed of cubic crystals, by specifying a set of basis functions. Taking the wire axis to be the z-direction, the simplest basis functions are powers of the Cartesian coordinates [13] in the lateral directions, such as

$$\Phi_\lambda(x, y, z) = \left(\frac{2x}{W}\right)^m\left(\frac{2y}{H}\right)^n \mathrm{e}^{\mathrm{i}qz} \tag{12}$$
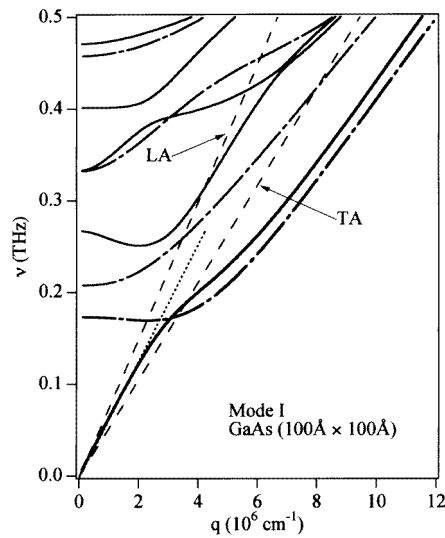
where $\lambda = (m, n)$, and q is the longitudinal wavevector of the acoustic phonon modes along the wire axis. W and H are the thicknesses of the wire in the x- and y-directions, respectively, with the origin being the wire axis at the centre of the cross section.

Substituting equation (12) into (9) and (10) yields the matrix elements

$$E_{i\lambda';j\lambda} = \delta_{i,j}\rho F(m + m'; n + n') \tag{13}$$

where

$$F(m; n) = \delta_{m,\mathrm{even}}\delta_{n,\mathrm{even}}\frac{1}{(m + 1)(n + 1)} \tag{14}$$

Figure 1. Dispersion curves of the dilatational phonon mode of a GaAs square wire with cross-sectional dimensions 100 Å × 100 Å. The solid and chain lines denote the dispersion curves of the mode with the vibrational patterns (a) and (b) in figure 4, respectively—see later. The dashed lines are the dispersion curves of the bulk LA and TA waves along the [001] direction. The dotted line is the dispersion curve of a longitudinal wave in a rod in the long-wavelength limit. The material parameters used are quoted from reference [21].

and $\Gamma_{i\lambda';\ell\lambda}$ given in appendix A.

We note here that another complete set of functions—products of the Legendre polynomials—are also useful as basis functions. The matrix **E** becomes diagonal in this case, since the Legendre polynomials are orthogonal, and equation (11) becomes the usual eigenvalue equation. Although the basis functions (12) are not orthogonal, they are linearly independent, and are related to the Legendre polynomials by a certain linear transformation. Hence, expanding the displacement in terms of the basis functions (12) is essentially equivalent to expanding them in terms of the Legendre polynomials. One advantage of using the basis functions (12) is the straightforward evaluation of the Γ and **E** matrix elements, irrespective of the wire's cross-sectional shape. Thus this method can deal with wires with a variety of cross-sectional shapes. Another advantage is that the basis functions (12) are useful for the classification of the phonon modes, as discussed below.

Table 1. A set of parities of the displacement components.

Phonon mode	u_x	u_y	u_z
I	$(-, +)$	$(+, -)$	$(+, +)$
II	$(-, -)$	$(+, +)$	$(+, -)$
III	$(+, +)$	$(-, -)$	$(-, +)$
IV	$(+, -)$	$(-, +)$	$(-, -)$

The basis functions have even or odd parity under inversion of the x- and/or y-coordinates. On expressing the parity of the basis function (12) by (μ, ν), where $\mu = (-1)^m$ and $\nu = (-1)^n$, the basis functions are classified into four parity groups, i.e. $(+, +)$, $(+, -)$,
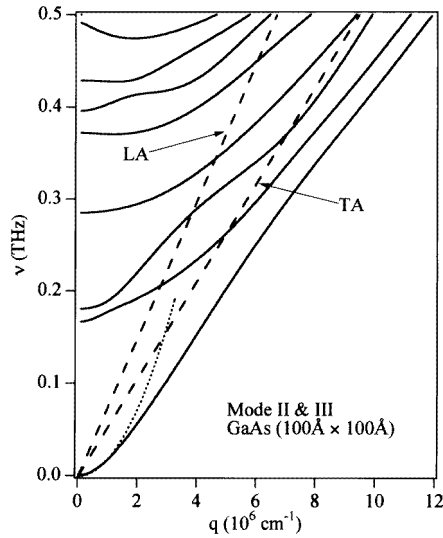
Figure 2. Dispersion curves of the flexural phonon modes of a GaAs square wire with cross-sectional dimensions 100 Å × 100 Å. The dispersion relations of the two flexural modes are degenerate for a square wire. The solid lines denote the dispersion curves, and the dashed lines are the dispersion curves of the bulk LA and TA waves along the [001] direction. The dotted line denotes the dispersion curve of a bending wave in a rod, showing the parabolic dispersion relation in the long-wavelength limit.

$(-, +)$, and $(-, -)$. The diagonal matrix elements $\Gamma_{i\lambda';i\lambda}$ connect basis functions belonging to the same parity group. In contrast, the off-diagonal matrix elements of $\Gamma_{i\lambda';j\lambda}$ connect basis functions with different parity. Thereby, each displacement component u_i consists of a set of basis functions belonging to one of the parity groups, and the displacement components u_x and u_y connected to the u_z with the parity (μ, ν) have parity $(-\mu, \nu)$ and $(\mu, -\nu)$, respectively. Normal phonon modes are described by combinations of these displacement components with different parities, and are classified into four kinds of vibrational mode with different spatial symmetries (see table 1). The displacement components for each mode, which we numbered I–IV for convenience, are given in appendix B.

We note that mode I is the dilatational mode, modes II and III are flexural modes, and mode IV is the torsional or shear mode, as can be understood from table 1 and equations (B1c), (B2c), (B3c), and (B4c). By considering the change of cross-sectional area for these modes, it is seen that only the dilatational mode is a compressional mode.

Although a large number of basis functions are needed for the exact expression of normal modes, a small number of basis functions are sufficient for the expression as far as low-frequency normal modes are concerned. The size of the truncated set of basis functions is limited by the maximum power N of the basis functions in equations (B1c), (B2c), (B3c), and (B4c), which is determined by studying the convergence of the dispersion relationships for the frequency range and cross-sectional dimensions of interest.

3. Dispersion relations

Figures 1, 2, and 3 illustrate the dispersion curves of the dilatational (I), flexural (II and III), and torsional and shear modes (IV), respectively, for a GaAs square wire with cross-sectional
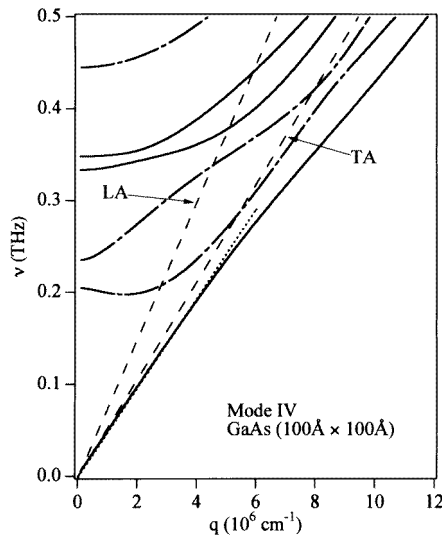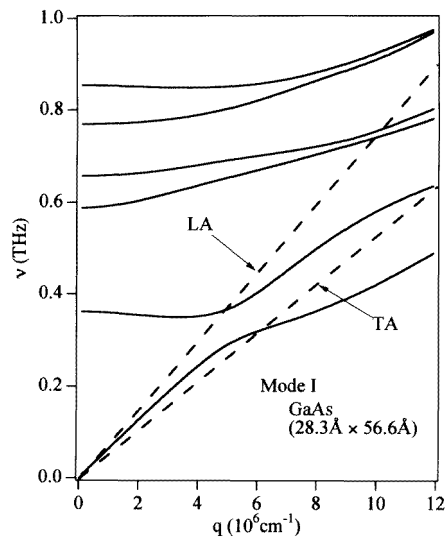
Figure 3. Dispersion curves of the torsional and shear phonon modes of a GaAs square wire with cross-sectional dimensions 100 Å × 100 Å. The solid and chain lines denote the dispersion curves of the torsional and shear modes, respectively. The dashed lines are the dispersion curves of the bulk LA and TA waves along the [001] direction. The dotted line is the dispersion curve of a torsional wave in a rod in the long-wavelength limit.

dimensions 100 Å × 100 Å, showing the phonon subband structures due to quantization of wavevectors in the lateral direction. For this size of wire, and a maximum frequency of 0.5 THz, N was determined empirically to be 12. The number of basis functions used for modes I, II, and III is 70, and for mode IV it is 63. It should be noted here that for square wires the dispersion relations of the two flexural modes are degenerate. For a small value of q, the lowest dispersion curves of the dilatational and torsional modes are proportional to q, while the flexural modes show a q^2-dependence. The parabolicity of the dispersion relations of the flexural modes stems from the fact that these modes are bending modes, similar to antisymmetric Lamb waves of a free plate [1], which can be analytically derived [17] in the long-wavelength limit as $\omega = q^2\sqrt{YI_i/\rho WH}$. Here Y is Young's modulus, and I_i is the moment of inertia of the cross section $I_x = H^3W/12$ about the x-axis for mode II and $I_y = HW^3/12$ about the y-axis for mode III. The parabolic dispersion relation denoted by the dotted curve in figure 2 reproduces the lowest dispersion curves of the flexural modes below $qW = 1$. On the other hand, the propagation velocity of the lowest subband of the dilatational mode is given by $\sqrt{Y/\rho}$, which is smaller than that of the bulk LA waves, $\sqrt{C_{11}/\rho}$. The dispersion curve in the long-wavelength limit is also plotted as the dotted line in figure 1. The propagation velocity of the torsional mode yields $v = \sqrt{G/\rho I_z}$, where G and I_z are the torsional rigidity and the moment of inertia of the cross section about the wire axis given by $I_z = I_x + I_y$, respectively. The dispersion curve is denoted by the dotted line in figure 3. Thus the lowest dispersion curves show the peculiarities of vibrational patterns of the normal modes.

For a larger q, or in a higher-frequency region, some dispersion curves of the dilatational mode intersect, which does not occur for the other modes. The intersection comes about because the dilatational mode consists of two independent modes: one is a simple dilatation and contraction as shown schematically in figure 4(a), whose displacement vector u is
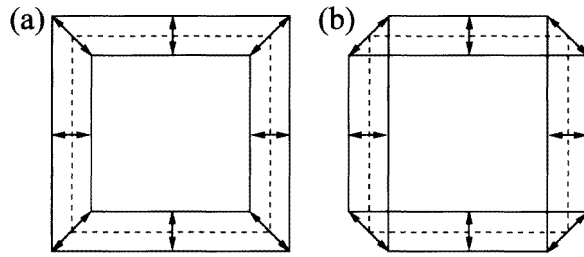
Figure 4. Schematic vibrational patterns of the dilatational mode: (a) the mode with the rotational symmetry $u = C_4u$ shows the simple dilatation and contraction of the wire, while (b) the mode with $u = -C_4u$ exhibits the alternate dilatation and contraction of the thickness of the wire. The squares with dashed lines denote the undeformed cross section of the wire, and the arrows denote the direction of displacement.
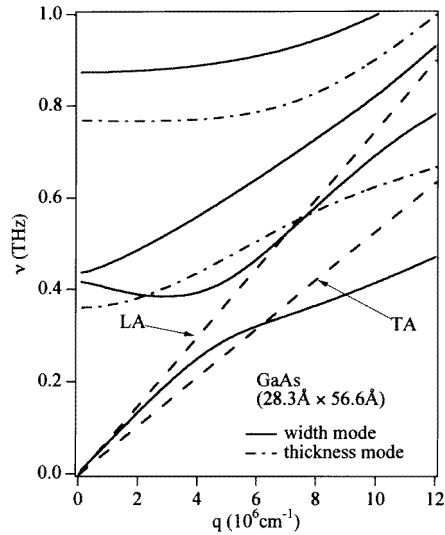

Figure 5. Dispersion curves of the dilatational phonon mode of a GaAs rectangular wire with cross-sectional dimensions 28.3 Å × 56.6 Å. The solid lines denote the dispersion curves, and the dashed lines are the dispersion curves of bulk LA and TA waves along the [001] direction.

transformed as $u = C_4u$, with rotation of the wire by $\pi/2$ about the wire axis, and the other is the alternating dilatation and contraction of the thickness of the wire in the x- and y-directions as shown in figure 4(b). The displacement vector is transformed as $u = -C_4u$ for the same rotational operation. These two modes are independent for a square wire, whose dispersion curves are denoted by the solid and chain lines in figure 1, respectively. The crossing of the dispersion curves is peculiar to square wires. These modes are no longer independent but are coupled for rectangular wires, inducing separation of their dispersion curves. Figure 5 shows the dispersion curves of the dilatational mode of a wire with cross-sectional dimensions 28.3 Å × 56.6 Å, which was discussed in reference [10], showing that all of the dispersion curves anticross at all of the frequencies studied.

Figure 6 shows the dispersion curves of the thickness and width modes of the wire. The lowest subband of the width mode is almost the same as that of the dilatational mode.

Figure 6. Dispersion curves of the thickness and width modes of a GaAs rectangular wire with cross-sectional dimensions 28.3 Å × 56.6 Å. The solid and chain lines denote the dispersion curves of the width and thickness modes, respectively. The dashed lines are the dispersion curves of the bulk LA and TA waves along the [001] direction.

The phonon modes of the rectangular wires have been believed to be well described by the approximate hybrid modes referred to as the thickness and width modes [15, 16], assuming separable boundary conditions—in particular, for wires with cross-sectional aspect ratios greater than two. We find poor agreement between the approximate hybrid modes and the dilatational mode for subbands other than the lowest. From these results, we conclude that the approximate hybrid modes are valid only for the lowest phonon subband.
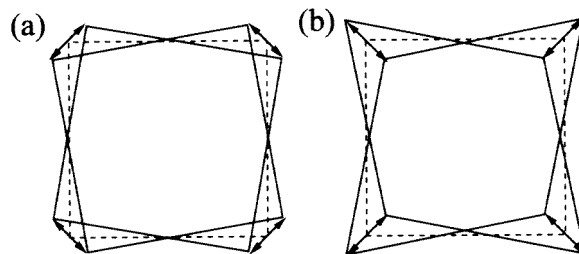
Figure 7. Schematic vibrational patterns of (a) the torsional mode with the rotational symmetry $u = C_4 u$ and (b) the shear mode with $u = -C_4 u$. The torsional mode shows rotation of the wire about the wire axis, and the shear mode exhibits alternating stretching in the two diagonal directions. The squares indicated with dashed lines denote the undeformed cross section of the wire, and the arrows denote the direction of the displacement.

Mode IV consists of the torsional and shear modes, as mentioned above. The vibrational patterns of these modes are schematically illustrated in figures 7(a) and 7(b), respectively. As can be understood from these figures, the displacement vector of the torsional mode is transformed as $u = C_4 u$ and that of the shear mode is transformed as $u = -C_4 u$ by rotation about the wire axis. Their dispersion relations are denoted in figure 3 by the solid

and chain lines, respectively. In contrast to the case for the dilatational mode, although these modes are independent for a square wire, there is no intersection of the dispersion curves, at least below 0.5 THz. These two modes are not well defined for rectangular wires, but are mixed. However, the effects of the mode mixing on the phonon subbands are expected to be small, since their dispersions are separated and there is no degeneracy between them for a square wire. On the other hand, the change in wire geometry modulates the mechanical properties of the wires, such as the torsional rigidity and the moments of inertia, causing modifications in the dispersion relations. As for the lowest subband, the dispersion curve is lowered with increasing aspect ratio, and can be approximated, at small q, by

$$\omega = \frac{2H}{W}\sqrt{\frac{\mu}{\rho}}q$$

for very flat rectangular wires, with $W \gg H$, where μ is one of the Lamé constants. In addition, change in the wire thickness affects the lateral wavevector quantization. Hence the dispersion relations of the higher subbands show a complicated dependence on the cross-sectional aspect ratio to a greater extent than do the lowest subbands.

As for the flexural modes, the dispersion relations of modes II and III are no longer degenerate for rectangular wires. The curvatures of the lowest subbands of modes II and III at small q are proportional to H and W, respectively. Interestingly, the dispersion relation of the lowest subband of mode II (III) depends, even for a large qW (H) (<10), only on H (W), as if the modes were Lamb waves in a free plate. In contrast, higher subbands are affected by the change in the lateral wavevector quantization as well as that in the mechanical properties of a wire, showing a complex dependence on the wire dimensions to a greater extent than do the lowest subbands like those of mode IV.

4. Edge modes

Figures 1, 2, and 3 show that the lowest and the following two dispersion curves of all of the modes fall below the dispersion curve of the bulk TA waves along the [001] direction with increasing q, which leads to complex lateral wavevectors. As a result, acoustic waves will decay exponentially in the directions normal to the edges or surfaces of the wires. Hence we may expect the existence of edge or surface modes for large q. To confirm that the vibrations are localized at the wire corners or surfaces, we investigated the spatial distribution of the squared displacement vectors $|\boldsymbol{u}|^2$. Figure 8(a) illustrates $|\boldsymbol{u}|^2$ for the lowest subband of the dilatational mode at $q = 8 \times 10^6$ cm^{-1} of the square wire with cross-sectional dimensions 100 Å $\times$ 100 Å, showing a conspicuously large amplitude at the wire corners. A large amplitude at the wire corners similar to that of figure 8(a) is also found for the second and third subbands of the dilatational mode, the lowest and second subbands of the flexural modes, and the lowest subbands of the torsional and shear modes. Figures 8(b) and 8(c) show $|\boldsymbol{u}|^2$ for the lowest subbands of the flexural and torsional modes at $q = 8 \times 10^6$ cm^{-1}. We refer to the modes with large amplitude at the corners as edge modes, although the amplitude does not completely vanish between the wire corners, in contrast to the case for edge modes localized at edges or steps of infinite crystals [18]. Completely localized vibrations at the wire corners are found for huge wires or for extremely large q.

In contrast to the case for the edge modes, we have not obtained any apparent evidence of surface modes, since the lowest subbands exhibit the characteristic decay of edge modes, as mentioned above. However, surface and edge modes should coexist for huge wires. Hence, some of the edge modes are expected to change into surface modes with increasing wire dimensions.
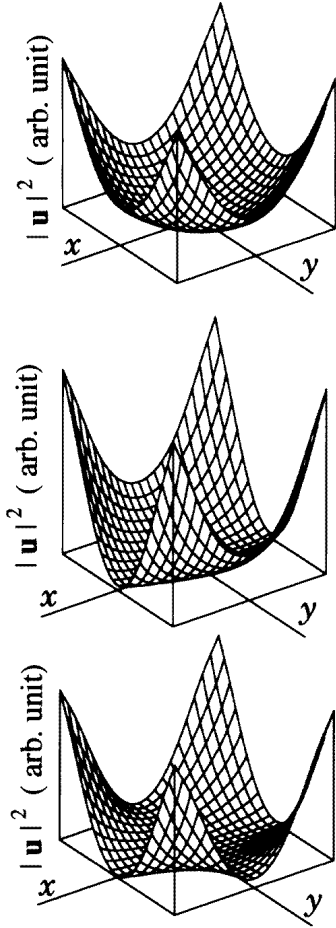
Figure 8. The spatial distribution of $|\boldsymbol{u}|^2$ for the lowest subband at $q = 8 \times 10^6$ cm^{-1} for the (a) dilatational, (b) flexural, and (c) torsional modes of a GaAs square wire of dimensions 100 Å × 100 Å.

5. The phonon field

The acoustic phonon field is described in terms of annihilation operators (a_J) and creation operators $(a_J^\dagger)$ of phonons as

$$\boldsymbol{u}_{op} = \sum_J \left[a_J \boldsymbol{u}_J + a_J^\dagger \boldsymbol{u}_J^* \right] \tag{15}$$

provided that the normal phonon modes $\boldsymbol{u}_J$ satisfy the orthonormal condition

$$\int_V \rho \boldsymbol{u}_{J'}^* \cdot \boldsymbol{u}_J \, \mathrm{d}V = \frac{\hbar \delta_{J,J'}}{2\omega_J} \tag{16}$$

as well as the completeness condition

$$\rho \sum_J \omega_J u_{J,i}(\boldsymbol{r}) u_{J,j}(\boldsymbol{r}') = \frac{\hbar}{2} \delta_{i,j} \delta(\boldsymbol{r} - \boldsymbol{r}'). \tag{17}$$

Here J denotes the phonon modes discussed above, the frequencies, and the longitudinal wavevectors.

The normal modes derived from equation (11) satisfy the orthogonality condition. Considering that $\boldsymbol{\Gamma}$ is a hermitian matrix and χ_J is an eigenvector of equation (11) for an eigenvalue ω_J^2, we obtain for two normal modes J and J'

$$(\omega_J^2 - \omega_{J'}^2)\chi_{J'}^{\dagger}\mathbf{E}\chi_J = 0. \tag{18}$$

For the non-degenerate case, $\omega_J \neq \omega_{J'}$, it is apparent that

$$\chi_{J'}^{\dagger}\mathbf{E}\chi_J = 0. \tag{19}$$

On substituting equation (6) into (16) and integrating over the volume, the left-hand side of equation (16) equals $V\chi_{J'}^{\dagger}\mathbf{E}\chi$. Hence the normal modes are orthogonal for the non-degenerate case. For the degenerate case, $\omega_J = \omega_{J'}$, we can demonstrate orthogonality, by considering the spatial symmetries of the normal modes. As an example, let us consider the case in which the dispersion curves of the dilatational modes intersect. As discussed above, the crossing of the dispersion curves occurs for a square wire, and the normal modes have distinct rotational symmetries along the wire axis, i.e. $\boldsymbol{u}_1 = C_4\boldsymbol{u}_1$ and $\boldsymbol{u}_2 = -C_4\boldsymbol{u}_2$. For the square wire, the following equality for an arbitrary function $f(\boldsymbol{r})$ holds:

$$\int_V f(\boldsymbol{r})\,\mathrm{d}\boldsymbol{r} = \int_V \left[C_4 f(\boldsymbol{r})\right]\,\mathrm{d}\boldsymbol{r}. \tag{20}$$

Because the product $\boldsymbol{u}_1\cdot\boldsymbol{u}_2$ changes its sign for the rotational operation C_4, the integral over the product $\boldsymbol{u}_1\cdot\boldsymbol{u}_2$ vanishes. Using the rotational symmetries and the parity of the normal modes, we can also demonstrate orthogonality among the four kinds of normal mode when their dispersion curves intersect, as for rectangular wires. Thus the orthogonality condition (16) is proved to be satisfied.

Putting $J = J'$, we obtain the normalization condition for the coefficients $\chi_{J,i\lambda}$ from equations (6) and (16):

$$\chi_J^{\dagger}\mathbf{E}\chi_J = \frac{1}{WHL_w}\frac{\hbar}{2\omega_J} \tag{21}$$

where L_w is the wire length. The coefficients $\chi_{J,i\lambda}$ should satisfy the normalization condition (21) as well as the eigenvalue equation (11) for the normalized phonon modes. In practice, the coefficients $\chi_{J,i\lambda}$ obtained numerically from equation (11) are scaled up or down so that they satisfy the normalization condition (21). Introducing a factor α (>0), we define the displacement components $u_{J,i}$ satisfying the normalization condition (16) by

$$u_{J,i} = \alpha\chi_{J,i\lambda}\Phi_\lambda \tag{22}$$

instead of (6). The factor α can be readily obtained by substituting equation (22) into (16), and the normalized displacement components $u_{J,i}$ are expressed by

$$u_{J,i} = \frac{1}{\sqrt{WHL_w}}\sqrt{\frac{\hbar}{2\omega_J}}\frac{\chi_{J,i\lambda}}{\sqrt{\chi_J^{\dagger}\mathbf{E}\chi_J}}\Phi_\lambda \tag{23}$$

in terms of the eigenvectors χ_J of equation (11) corresponding to the normal modes.

In contrast to the case for the orthogonality condition, it is difficult to prove the completeness of the normal modes in terms of the solutions of equation (11). However, completeness should be satisfied if all of the normal modes are included in the summation of equation (17). In this work, we have investigated all possible phonon modes with spatial symmetries related to a rectangular wire. We have confirmed the expected bulk modes and have identified a previously overlooked edge mode. Therefore we anticipate that the normal modes obtained in this paper satisfy the completeness condition (17).

Thus the phonon field can be expressed in terms of the normalized phonon modes (23) and their complex conjugates. The Hamiltonian of the phonons is diagonalized using equations (15) and (23). These two equations can also be used to derive the deformation and piezoelectric potential Hamiltonians, and the ripple mechanism [19, 20], as will be discussed elsewhere.

6. Summary

The acoustic phonon modes of Q1D rectangular wires composed of cubic crystals have been precisely derived by using the xyz-algorithm used in resonant ultrasound spectroscopy. The acoustic phonon modes are classified according to their spatial symmetries into a compressional mode termed the dilatational mode and non-compressional modes referred to as the torsional, shear, and two flexural modes. The dispersion relations of the normal modes were obtained for GaAs square and rectangular wires, exhibiting subband structures. The lowest subbands of these modes reduce to the vibrational modes of a rod in the long-wavelength limit, showing linear or parabolic dispersion relations with respect to a longitudinal wavevector q peculiar to each mode. There are intersections among the dispersion relations of the dilatational mode because the dilatational mode is divided into two independent modes for square wires. For a rectangular wire, mode coupling between the dilatational modes and between the torsional and shear modes take place. The mode coupling substantially modifies the dispersion relations of the dilatational mode, separating their dispersion curves, while the coupling between the torsional and shear modes does not have significance for phonon spectra, unlike the change in mechanical properties. We also examined the validity of the approximate hybrid modes by comparing the dispersion relations for a rectangular wire, and found that only the lowest subband can be well described by the width mode. We confirm that the lowest subbands are the acoustic edge modes which decay in the directions normal to the wire corners. Finally, applying the normalization condition to the phonon modes, we formulated the phonon field.

In this paper we have demonstrated that the acoustic phonon modes of Q1D wires with square and rectangular cross sections can be precisely derived. The method used is general, and can be applied to free-standing structures with other cross-sectional profiles, for instance triangular [6]. Experimental evidence for reduced-dimensionality phonons has been reported for supported metal wires [7, 8]. The coupling of such wires to a substrate will cause the phonon spectrum to be different from that of the free-standing wires reported here. We anticipate that, with some modification, the xyz-algorithm will be applicable to supported structures, which will enable a comparison to be made between the predicted and observed phonon spectra. Work towards this application is under way, and will be reported elsewhere.

Acknowledgments

Appendix A. The matrix Γ

The matrix elements $\Gamma_{i\lambda';j\lambda}$ are

$$\Gamma_{1\lambda';1\lambda} = \frac{4}{W^2}C_{11}mm'F(m+m'-2;n+n') + \frac{4}{H^2}C_{44}nn'F(m+m';n+n'-2)$$
$$+ C_{44}q^2F(m+m';n+n') \tag{A1}$$

$$\Gamma_{1\lambda';2\lambda} = \frac{4}{WH}(C_{12}m'n + C_{44}mn')F(m+m'-1;n+n'-1) \tag{A2}$$

$$\Gamma_{1\lambda';3\lambda} = -\frac{2i}{W}q(C_{44}m - C_{12}m')F(m+m'-1;n+n') \tag{A3}$$

$$\Gamma_{2\lambda';1\lambda} = \frac{4}{WH}(C_{44}m'n + C_{12}mn')F(m+m'-1;n+n'-1) \tag{A4}$$

$$\Gamma_{2\lambda';2\lambda} = \frac{4}{W^2}C_{44}mm'F(m+m'-2;n+n') + \frac{4}{H^2}C_{11}nn'F(m+m';n+n'-2)$$
$$+ C_{44}q^2F(m+m';n+n') \tag{A5}$$

$$\Gamma_{2\lambda';3\lambda} = -\frac{2i}{H}q(C_{44}n - C_{12}n')F(m+m';n+n'-1) \tag{A6}$$

$$\Gamma_{3\lambda';1\lambda} = -\frac{2i}{W}q(C_{12}m - C_{44}m')F(m+m'-1;n+n') \tag{A7}$$

$$\Gamma_{3\lambda';2\lambda} = -\frac{2i}{H}q(C_{12}n - C_{44}n')F(m+m';n+n'-1) \tag{A8}$$

$$\Gamma_{3\lambda';3\lambda} = \frac{4}{W^2}C_{44}mm'F(m+m'-2;n+n') + \frac{4}{H^2}C_{44}nn'F(m+m';n+n'-2)$$
$$+ C_{11}q^2F(m+m';n+n'). \tag{A9}$$

Appendix B. Displacement components

The displacement components are

$$u_x = \sum_{r,s=0}^{2(r+s)+1\leqslant N} \chi_{1rs}\left(\frac{2x}{W}\right)^{2r+1}\left(\frac{2y}{H}\right)^{2s} e^{iqz} \tag{B1a}$$

$$u_y = \sum_{r,s=0}^{2(r+s)+1\leqslant N} \chi_{2rs}\left(\frac{2x}{W}\right)^{2r}\left(\frac{2y}{H}\right)^{2s+1} e^{iqz} \tag{B1b}$$

$$u_z = \sum_{r,s=0}^{2(r+s)\leqslant N} \chi_{3rs}\left(\frac{2x}{W}\right)^{2r}\left(\frac{2y}{H}\right)^{2s} e^{iqz} \tag{B1c}$$

for mode I,

$$u_x = \sum_{r,s=0}^{2(r+s)+2\leqslant N} \chi_{1rs}\left(\frac{2x}{W}\right)^{2r+1}\left(\frac{2y}{H}\right)^{2s+1} e^{iqz} \tag{B2a}$$

$$u_y = \sum_{r,s=0}^{2(r+s)\leqslant N} \chi_{2rs}\left(\frac{2x}{W}\right)^{2r}\left(\frac{2y}{H}\right)^{2s} e^{iqz} \tag{B2b}$$

$$u_z = \sum_{r,s=0}^{2(r+s)+1\leqslant N} \chi_{3rs}\left(\frac{2x}{W}\right)^{2r}\left(\frac{2y}{H}\right)^{2s+1} e^{iqz} \tag{B2c}$$

for mode II,

$$u_x = \sum_{r,s=0}^{2(r+s)\leqslant N} \chi_{1rs} \left(\frac{2x}{W}\right)^{2r} \left(\frac{2y}{H}\right)^{2s} e^{iqz} \tag{B3a}$$

$$u_y = \sum_{r,s=0}^{2(r+s)+2\leqslant N} \chi_{2rs} \left(\frac{2x}{W}\right)^{2r+1} \left(\frac{2y}{H}\right)^{2s+1} e^{iqz} \tag{B3b}$$

$$u_z = \sum_{r,s=0}^{2(r+s)+1\leqslant N} \chi_{3rs} \left(\frac{2x}{W}\right)^{2r+1} \left(\frac{2y}{H}\right)^{2s} e^{iqz} \tag{B3c}$$

for mode III, and

$$u_x = \sum_{r,s=0}^{2(r+s)+1\leqslant N} \chi_{1rs} \left(\frac{2x}{W}\right)^{2r} \left(\frac{2y}{H}\right)^{2s+1} e^{iqz} \tag{B4a}$$

$$u_y = \sum_{r,s=0}^{2(r+s)+1\leqslant N} \chi_{2rs} \left(\frac{2x}{W}\right)^{2r+1} \left(\frac{2y}{H}\right)^{2s} e^{iqz} \tag{B4b}$$

$$u_z = \sum_{r,s=0}^{2(r+s)+2\leqslant N} \chi_{3rs} \left(\frac{2x}{W}\right)^{2r+1} \left(\frac{2y}{H}\right)^{2s+1} e^{iqz} \tag{B4c}$$

for mode IV.

References

[1] Auld B A 1973 *Acoustic Fields and Waves in Solids* vol II (New York: Wiley) ch 10
[2] Kelly M J 1982 *J. Phys. C.: Solid State Phys.* **15** L969
[3] Ishii K 1973 *Prog. Theor. Phys. Suppl.* **53** 77
[4] Smith C G and Wybourne M N 1986 *Solid State Commun.* **57** 411
[5] Jäckle J 1981 *Solid State Commun.* **39** 1261
[6] Potts A, Kelly M J, Smith C G, Hasko D G, Cleaver J R A, Ahmed H, Peacock D C, Ritchie D A, Frost J E F
    and Jones G A C 1990 *J. Phys.: Condens. Matter* **2** 1817
[7] Seyler J and Wybourne M N 1992 *Phys. Rev. Lett.* **69** 1427
[8] Wybourne M N 1996 *Physica* B **219+220** 13
[9] Nishiguchi N 1995 *Phys. Rev.* B **52** 5279
[10] Segi Y, Kim K W, Stroscio M A, Iafrate G J and Ballato A 1994 *Phys. Rev.* B **50** 1733
[11] Bannov N A, Mitin V V and Stroscio M A 1995 *Quantum Transport in Ultrasmall Devices* ed D K Ferry,
    H L Grubin, C Jacoboni and A-P Jauho (New York: Plenum) p 191
[12] Demarest H H Jr 1971 *J. Acoust. Soc. Am.* **49** 768
[13] Visscher W M, Migliori A, Bell T M and Reinert R A 1991 *J. Acoust. Soc. Am.* **90** 2154
[14] Maynard J 1996 *Phys. Today* **49** (1) 26, and references quoted therein
[15] Morse R W 1948 *J. Acoust. Soc. Am.* **20** 833
[16] Morse R W 1950 *J. Acoust. Soc. Am.* **22** 219
[17] Landau L D, Lifshitz E M, Kosevich A M and Pitaevskii L P 1986 *Theory of Elasticity* 3rd edn (New York:
    Pergamon) ch 12
[18] Maradudin A A, Wallis R F, Mills D L and Ballard R L 1972 *Phys. Rev.* B **6** 1106
[19] Vasko F T and Mitin V V 1995 *Phys. Rev.* B **52** 1500
[20] Knipp P A and Reinecke T L 1995 *Phys. Rev.* B **52** 5923
[21] Adachi S 1985 *J. Appl. Phys.* **58** R1